ACS APPLIED MATERIALS & INTERFACES

Research Article

Cite This: ACS Appl. Mater. Interfaces 2018, 10, 40890−40900

www.acsami.org

Quaternary Ammonium-Terminated Films Formed from Mixed Bidentate Adsorbates Provide a High-Capacity Platform for Oligonucleotide Delivery

Johnson Hoang,[†] Chul Soon Park,[‡] Han Ju Lee,[‡] Maria D. Marquez,[‡] Oussama Zenasni,[‡] Preethi H. Gunaratne,*[,†] and T. Randall Lee*[,‡]

[†]Department of Biology and Biochemistry, University of Houston, Houston, Texas 77204-5001, United States

[‡]Departments of Chemistry and Chemical Engineering and the Texas Center for Superconductivity, University of Houston, Houston, Texas 77204-5003, United States

Supporting Information

ABSTRACT: The exposure of quaternary ammonium groups on surfaces allows self-assembled monolayers (SAMs) to serve as architectural platforms for immobilizing oligonucleotides. The current study describes the preparation of SAMs derived from four unique bidentate adsorbates containing two different ammonium termini (i.e., trimethyl- and triethyl-) and comparison to their monodentate analogs. Our studies found that SAMs derived from the bidentate adsorbates offered considerable enhancements in oligonucleotide binding when compared to SAMs derived from their monodentate analogs. The generated SAMs were analyzed using ellipsometry, X-ray photoelectron spectroscopy, contact angle goniometry, polarization modulation infrared reflection-absorption spectroscopy, and electrochemical quartz crystal microbalance. These analyses showed that the immobilization of oligonucleotides was affected by changes in the terminal functionalities and the relative packing densities of the monolayers. In efforts to enhance further the immobilization of oligonucleotides on these SAM surfaces, we explored the use of adsorbates having aliphatic linkers with systematically varying chain lengths to form binary SAMs on gold. Mixed monolayers with 50:50 ratios of adsorbates showed the greatest oligonucleotide binding. These studies lay the groundwork for oligonucleotide delivery using gold-based nanoparticles and nanoshells.

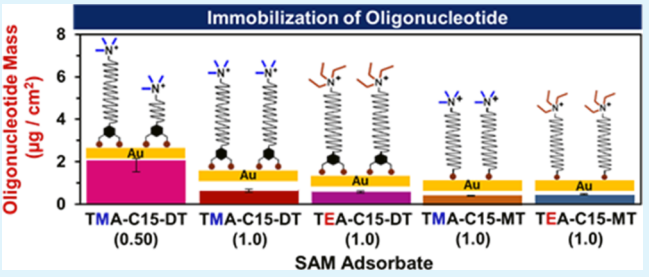

KEYWORDS: *self-assembled monolayer, oligonucleotide delivery, quaternary ammonium, single-stranded DNA, binary-mixed SAMs*

INTRODUCTION

The functionalization of surfaces with charged coatings constitutes a well-established strategy to tailor the interactions between surfaces and various types of contacting matter. For example, surfaces functionalized with zwitterionic termini often serve as foul-resistant surfaces.[1−3] Furthermore, amino-terminated surfaces can be used to bind molecules of DNA for sensing and therapeutic applications.[4−6] Self-assembled monolayers (SAMs) provide a prominent architectural platform for designing functionalized surfaces; the resultant organic thin films are formed via the spontaneous adsorption of amphiphilic molecules on the surfaces of a variety of coinage metals (e.g., copper, gold, palladium, and silver).[7] A specific class of SAMs consists of adsorbates containing a sulfur headgroup chemisorbed on gold surfaces due to the high affinity of sulfur to gold.[7,8] Furthermore, the formed films on the substrate can provide an appropriate platform for the exposure and utilization of the terminal functional group (tailgroup) of the SAM. This methodology allows for a variety of terminal functional groups (e.g., amine,[8−10] carboxylic acid,[11,12] and thiol[13]) to form a framework that allows for the direct fixation of ligands (e.g., nucleotides and proteins) via post-modification of the SAMs.[14−17] Thus, the outcome allows for further advancement and development in a variety of applications, such as microarrays,[18] protein chips,[19,20] colorimetric sensors,[21] and biosensors.[22]

The formation of SAMs possessing ammonium termini has been explored for the purpose of generating surfaces for biological applications via electrostatic interactions with biomolecules.[17] The ammonium terminal group introduces a polar and charged functionality that allows biomolecules to interact electrostatically and bind onto the surface.[23−25] However, many of the targeted applications involving ammonium-terminated SAMs have been hindered due to: (i) the oxidation of the terminal amine groups,[26] (ii) the susceptibility of the ammonium groups to changes in the pH of the environment,[26] and (iii) the interaction between amine moieties and the surface of the gold.[26] In contrast, the use of quaternary ammonium termini can often circumvent these problems; however, the incorporation of quaternary ammo-

Received: July 20, 2018
Accepted: October 18, 2018
Published: October 18, 2018

DOI: 10.1021/acsami.8b12244
ACS Appl. Mater. Interfaces 2018, 10, 40890−40900

nium termini in organic thin films has led to increases in the lateral spacing of the terminal groups, which exposes the underlying aliphatic spacer,[27] giving rise to additional degrees of freedom for aliphatic chain movement within the SAMs. The enhanced terminal group spacing and chain mobility within these SAMs provide a means for the intercalation of molecules into the monolayer structure.[28] Moreover, these characteristics allow for the formation of low-density SAMs with diminished hydrophobicity for the intercalation of biomolecules.[28]

In this report, we describe the synthesis of two series of quaternary ammonium-terminated adsorbates, one having the customary monodentate headgroup and the other having a unique bidentate headgroup (Figure 1), for generating films

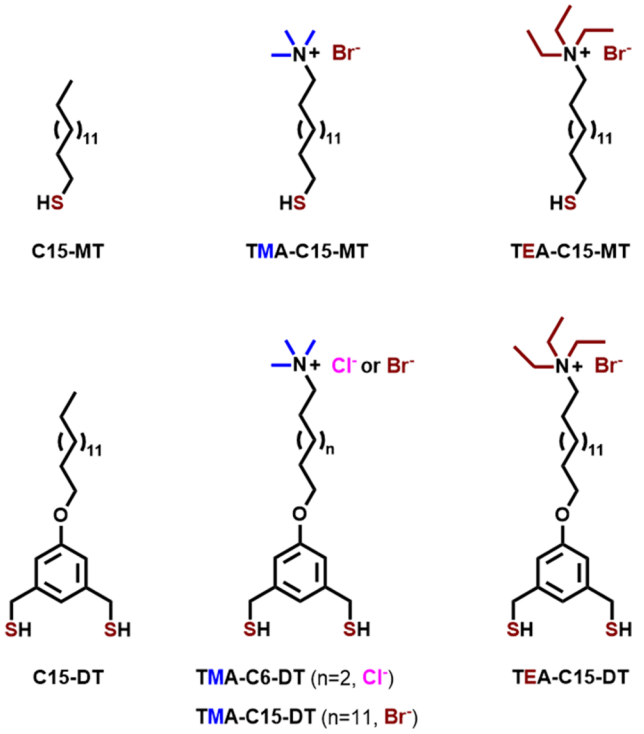

Figure 1. Molecular structures of the adsorbates used to generate methyl-terminated SAMs (**C15-MT** and **C15-DT**) and their trialkylammonium-terminated counterparts (**TMA-C15-MT**, **TEA-C15-MT**, **TMA-C6-DT**, **TMA-C15-DT**, and **TEA-C15-DT**).

with enhanced stability.[29] The three monodentate adsorbates contain either trimethylammonium termini (15-mercapto-*N*,*N*,*N*-trimethylpentadecan-1-ammonium; **TMA-C15-MT**) or triethylammonium termini (*N*,*N*,*N*-triethyl-15-mercaptopentadecan-1-ammonium; **TEA-C15-MT**) and octadecanethiol (**ODT**) as a standard. This series of adsorbates allows a direct comparison between the bidentate adsorbates containing the trimethylamine-terminated 15-(3,5-bis(mercaptomethyl)phenoxy)-*N*,*N*,*N*-trimethylpentadecan-1-ammonium (**TMA-C15-DT**) and 6-(3,5-bis(mercaptomethyl)phenoxy)-*N*,*N*,*N*-trimethylhexan-1-ammonium (**TMA-C6-DT**), as well as the triethylamine-terminated 15-(3,5-bis(mercaptomethyl)phenoxy)-*N*,*N*,*N*-triethylpentadecan-1-ammonium (**TEA-C15-DT**) and the standard (5-(pentadecyloxy)-1,3-phenylene)dimethanethiol (**C15-DT**). Herein, we investigate (1) the effects of increasing the lateral spacing of the terminal groups, (2) the effects of enhanced film stability, and (3) the effect of these phenomena on the nucleotide loading capacity on the surfaces. These studies provide the foundation for therapeutic oligonucleotide delivery using gold-based nanoparticles[17,30−32] and nanoshells,[33−35] where the latter nanostructures can be activated by tissue-transparent near-infrared light.[34,36]

RESULTS AND DISCUSSION

Single-Component Self-Assembled Monolayer Films.

Measurements of Film Thickness. Analysis of the films using ellipsometry provides an assessment on the film thickness following the chemisorption and equilibration of the adsorbate on the gold substrate.[8,37] Table 1 shows the measured film

Table 1. Ellipsometric Thicknesses, Relative Packing Densities, and Bound Sulfur Contents of the SAMs Formed from Each Adsorbate

adsorbate	ellipsometric thickness (Å)	relative packing density (%)	percentage of bound sulfur (%)
ODT	23 ± 1	100	100
C15-MT	19 ± 2	97 ± 2	98 ± 1
TMA-C15-MT	18 ± 1	86 ± 3	97 ± 1
TEA-C15-MT	19 ± 1	74 ± 6	89 ± 4
C15-DT	20 ± 1	49 ± 2	85 ± 3
TMA-C15-DT	22 ± 1	47 ± 2	82 ± 3
TEA-C15-DT	23 ± 1	44 ± 2	80 ± 3

thicknesses for the SAMs derived from **ODT**, **C15-MT**, **TMA-C15-MT**, **TEA-C15-MT**, **C15-DT**, **TMA-C15-DT**, and **TEA-C15-DT**; for reference, we calculated the lengths of the adsorbates in their trans-extended conformations (see Figures S1a,b in the Supporting Information). Monolayers generated from **ODT**, **C15-MT**, and **TMA-C15-MT** have thicknesses of 23, 19, and 18 Å, respectively. These results are comparable to the thicknesses of structurally related monodentate SAMs studied previously.[28,39] Similarly, films derived from **TEA-C15-MT** show an average thickness of 19 Å, where the negligible increase perhaps reflects the additional methylene units in the ammonium tailgroup compared to SAMs derived from **TMA-C15-MT**. In comparison, the bidentate SAM derived from **C15-DT** has a thickness of 20 Å, which is similar to the previously reported value,[39] while those derived from **TMA-C15-DT** and **TEA-C15-DT** have thicknesses of 22 and 23 Å, respectively. The latter observed increase in thickness can be rationalized by the added size increase of the bulky ammonium termini. While charge−charge repulsion between the quaternary ammonium-terminated adsorbates can plausibly inhibit the packing densities (and correspondingly diminish the measured thicknesses), our obtained thickness values appear to be unaffected by this interaction. The similar measure of ellipsometric thicknesses for the charged surfaces and the non-charged surfaces can be attributed to both the strong covalent S−Au binding of the adsorbates to the surface of gold and the existence of a hydration layer for the charged surfaces; notably, the existence of a hydration layer for charged SAMs on gold has been described in the literature.[40]

Analysis of the SAMs by X-ray Photoelectron Spectroscopy (XPS). Analysis of the SAMs by XPS provides essential information on the chemical composition and oxidation state of various elements that make up organic layers. Figure 2 shows the XPS spectra of the binding energy regions for the S 2p, Br 3d, N 1s, and C 1s core electrons in the SAMs.

DOI: 10.1021/acsami.8b12244
ACS Appl. Mater. Interfaces 2018, 10, 40890−40900

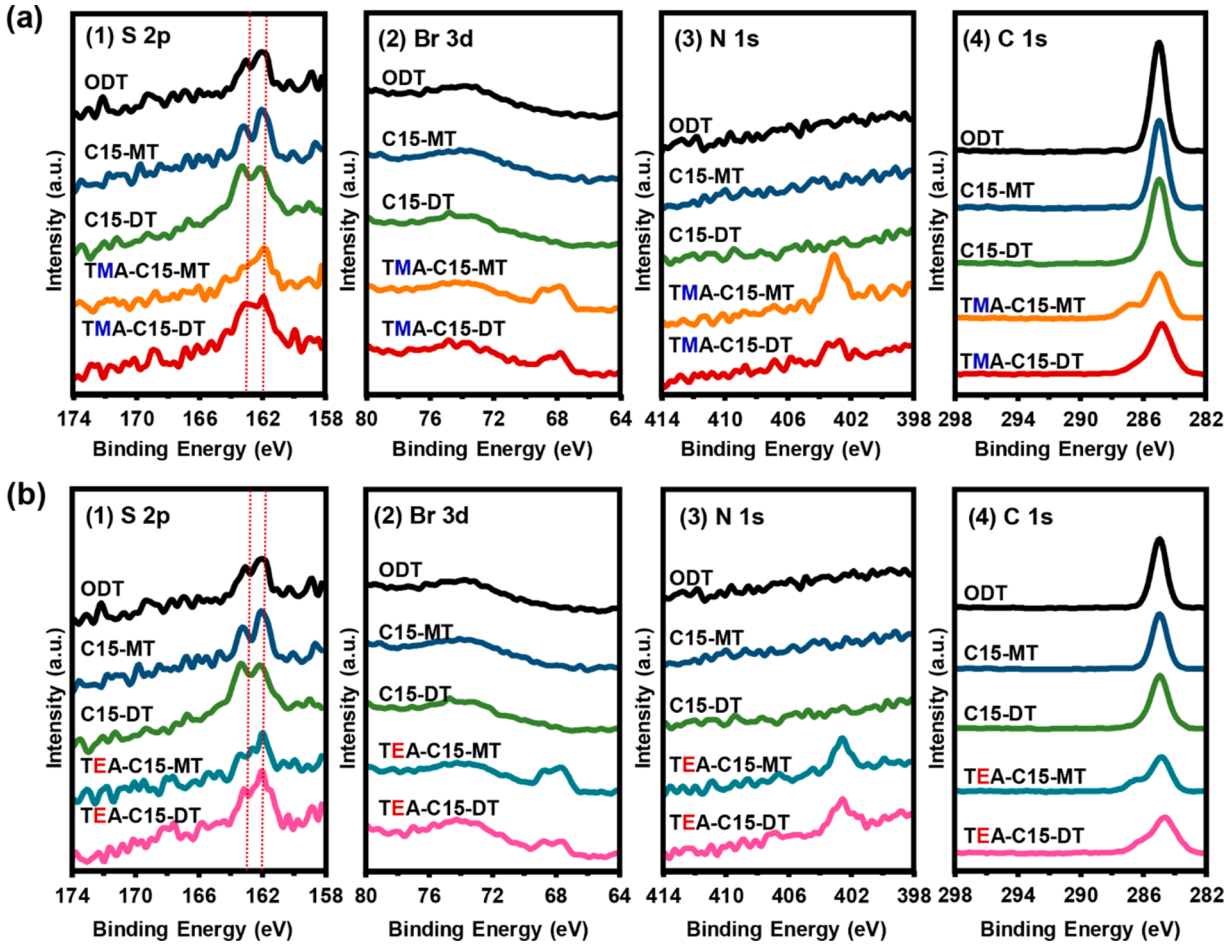

Figure 2. XPS spectra for the (a) trimethylammonium-terminated SAMs (**TMA-C15-MT** and **TMA-C15-DT**) and (b) the triethylammonium-terminated SAMs (**TEA-C15-MT** and **TEA-C15-DT**) for the (1) S 2p, (2) Br 3d, (3) N 1s, and (4) C 1s regions. The SAMs generated from the methyl-terminated adsorbates (**ODT**, **C15-MT**, and **C15-DT**) are included in both panels for comparison.

Separately, the binding energy regions of the Au $4f_{7/2}$ electrons, which are used as a reference for calibrating the XPS signal intensities, are shown in Figures S2a,b.

Analysis of the S 2p region (Figures 2a1,b1) for the SAMs reveals peaks associated with bound thiols corresponding to the S $2p_{3/2}$ and S $2p_{1/2}$ electrons at ∼162 and ∼163 eV.[7,9,41,42] The absence of peaks at ∼164−165 eV and ∼168 eV, which correspond to unbound thiol and oxidized sulfur species, confirms that the majority of the thiols are bound to the gold surface.[7,9,41] Moreover, to calculate the amount of bound thiol on the substrates (given in Table 1 and shown in parentheses here), deconvolutions of the S 2p peaks (Figures S3 and S4) were performed for the SAMs derived from **ODT** (100%), **C15-MT** (98%), **TMA-C5-DT** (97%), **TEA-C15-DT** (89%), **C15-DT** (85%), **TMA-C15-DT** (82%), and **TEA-C15-DT** (80%).

The Br 3d signals (Figures 2a2,b2) convey spin−orbit splitting for the SAMs derived from **TMA-C15-MT**, **TEA-C15-MT**, **TMA-C15-DT**, and **TEA-C15-DT** with characteristic binding energies for the $3d_{3/2}$ electrons (68.9, 68.7, 68.5, and 68.8 eV, respectively) and $3d_{5/2}$ electrons (67.9, 67.7, 67.6, and 67.7, respectively).[27] The presence of the bromine peaks can be attributed to the counterions present in the quaternary ammonium-terminated SAMs (**TMA-C15-MT**, **TEA-C15-MT**, **TMA-C15-DT**, and **TEA-C15-DT**), which is consistent with the synthetic approach used to prepare the adsorbates. Similarly, the presence of the N 1s signal at ∼403 eV in Figures 2a3,b3 can be attributed to the ammonium groups in these SAMs.[27] In addition, the O 1s peak at ∼532.5 eV, shown in Figure S5, for the bidentate SAMs derived from **C15-DT**, **TMA-C15-DT**, and **TEA-C15-DT** can be attributed to their phenoxy framework. Notably, O 1s peaks at a lower binding energy (∼531.5 eV) were also detected in the SAMs derived from the monodentate quaternary ammonium-terminated adsorbates, **TMA-C15-MT** and **TEA-C15-MT**, but not found in the SAMs derived from **ODT** and **C15-MT**. These O 1s peaks plausibly arose from a hydration layer on the surface of the quaternary ammonium-terminated SAMs.[40]

The dominating peak in the C 1s region (Figures 2a4,b4) is that corresponding to the methylene carbons at ∼285 eV.[27] The protruding shoulder at ∼286 eV, which is only present in the quaternary ammonium-terminated SAMs, corresponds to the C−N group.[27] Furthermore, the C−O carbon, present in the bidentate SAMs, exhibits a peak at ∼286.6 eV.[43,44] We performed a more quantitative analysis to determine the relative packing densities of these adsorbates by obtaining the sulfur-to-gold (S/Au) ratios from the XPS spectra. For our analysis, **ODT** was used as a reference SAM. SAMs generated from **ODT** on Au(111) surfaces have been reported to form well-ordered and densely packed films with a $(\sqrt{3} \times \sqrt{3})R30°$ overlayer, which when characterizing films generated from new adsorbates serves as an excellent point of reference.[7,8,37,45,46]

DOI: 10.1021/acsami.8b12244
ACS Appl. Mater. Interfaces 2018, 10, 40890−40900

The analysis was performed with the assumptions that (1) **ODT** forms a well-ordered and densely packed SAM on gold and (2) **ODT** SAMs possess 100% bound thiols. The calculated ratios are displayed in Table 1. The adsorbates exhibited packing densities of 97, 86, 74, 49, 47, and 44% for **C15-MT**, **TMA-C15-MT**, **TEA-C15-MT**, **C15-DT**, **TMA-C15-DT**, and **TEA-C15-DT**, respectively. The lower packing density of the SAMs generated from the quaternary ammonium-terminated adsorbates, compared to the non-charged analogs, can perhaps be attributed to repulsive charge−charge interactions between the quaternary ammonium termini.

Wettability of the SAMs. The wettability of the surfaces was probed with the polar protic solvent water. Surfaces that exhibit an advancing contact angle measurement lower than 90° are generally considered wettable surfaces, with those having a higher contact angle being non-wettable.[47] Figure 3

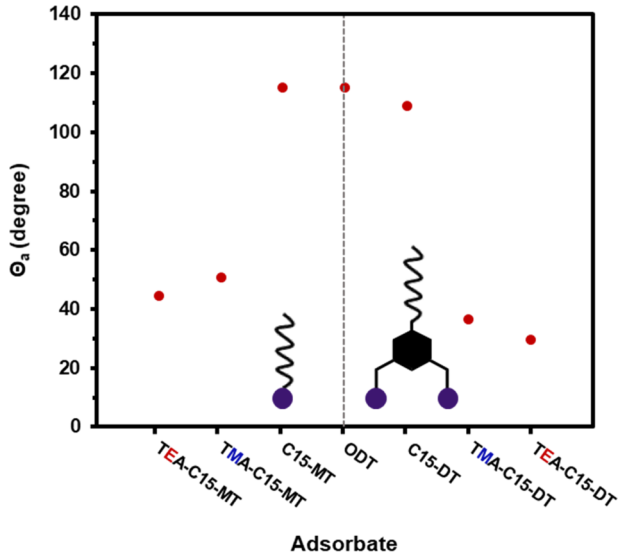

Figure 3. Advancing contact angles of water on the SAMs generated from **ODT**, **C15-MT**, **TMA-C15-MT**, **TEA-C15-MT**, **C15-DT**, **TMA-C15-DT**, and **TEA-C15-DT**. Error bars that are not visible fall within the symbol.

and Table S1 show the advancing contact angles of water for all of the SAMs. The contact angles obtained for the monodentate methyl-terminated SAMs, **ODT** and **C15-MT**, were 115°, in accordance with the literature values.[48,49] Compared to the monodentate analogs, the bidentate methyl-terminated SAM, **C15-DT**, showed a lower advancing contact angle of 109°, which is consistent with a film having chains that are less densely packed, exposing some fraction of methylene groups at the interface.[39]

The SAMs derived from the monodentate ammonium-terminated SAMs, **TMA-C15-MT** and **TEA-C15-MT**, have lower contact angle values at 51 and 45°, respectively, than the corresponding methyl-terminated SAMs, **ODT** and **C15-MT**. The lower values can be attributed to the presence of the hydrophilic ammonium terminal group in these SAMs.[1,50] Moreover, the contact angles of the SAM derived from **TMA-C15-MT** were found to be slightly higher than those on the SAM derived from **TEA-C15-MT**. This observation can be attributed to the increased steric bulk of the triethylammonium vs the trimethylammonium at the SAM−liquid interface. The larger terminal group plausibly decreases the packing density of the film and correspondingly increases the wettability, an observation also supported by the XPS analysis (vide supra).

Comparatively, the SAMs derived from the bidentate adsorbates, **TMA-C15-DT** and **TEA-C15-DT**, showed lower contact angles than the corresponding methyl-terminated adsorbate, **C15-DT**, with values of 37° and 30°, respectively. Similar to the monodentate SAMs, the wettability of the triethylammonium-terminated SAM is greater than the trimethylammonium-terminated SAM. The triethylammonium-terminated SAM derived from the bidentate adsorbate, **TEA-C15-DT**, showed a lower contact angle value than the corresponding trimethylammonium-terminated analog, **TMA-C15-DT**. As previously discussed, and supported by the calculated packing densities, the steric bulk of the triethylammonium group plausibly causes a decrease in the packing density of the films, which makes them more wettable. Overall, the data obtained from the contact angles of water indicate that the wettability of the SAMs follows the order of: **ODT** = **C15-MT** > **C15-DT** ≫ **TMA-C15-MT** > **TEA-C15-MT** > **TMA-C15-DT** > **TEA-C15-DT**.

Analysis of the SAMs by Polarization Modulation Infrared Reflection-Absorption Spectroscopy (PM-IRRAS). To evaluate the conformational order of the SAMs, we performed an analysis of the symmetric ($\nu_s^{CH_2}$) and antisymmetric ($\nu_a^{CH_2}$) C−H stretching of the methylene units using PM-IRRAS.[9,41] The conformational order of a film can be estimated by the position of the latter two bands.[51] Films with a $\nu_a^{CH_2}$ at 2918 cm^{-1} are indicative of a mostly trans-extended alkyl chain, a key characteristic of a well-ordered film, whereas a shift to a higher wavenumber indicates a film with diminished conformational order.[51] The PM-IRRAS spectra of the C−H stretching region for the SAMs are shown in Figure S6. The $\nu_a^{CH_2}$ for the SAMs derived from **ODT** and **C15-MT** appeared at 2918 cm^{-1}, indicating a well-ordered film. Furthermore, the position of the $\nu_a^{CH_2}$ of the SAMs derived from **TMA-C15-MT**, **TEA-C15-MT**, **C15-DT**, **TMA-C15-DT**, and **TEA-C15-DT** appeared at 2922, 2923, 2926, 2926, and 2927 cm^{-1}, respectively. In this aspect, all quaternary ammonium-terminated SAMs (**TMA-C15-MT**, **TEA-C15-MT**, **TMA-C15-DT**, and **TEA-C15-DT**) and the SAM derived from the methyl-terminated dithiol (**C15-DT**) showed disorder in the alkyl chains, with the bidentate quaternary ammonium SAMs showing the greatest degree of disorder. The disorder in the films can be attributed to the formation of a loosely packed SAM due to the sterically bulky terminal groups.

We note also that the C−H stretches originating from the CH_3 group of the quaternary ammonium SAMs (**TMA-C15-MT**, **TEA-C15-MT**, **TMA-C15-DT**, and **TEA-C15-DT**) and the **C15-DT** SAM are either very weak or undetectable in the spectra. The absence of methyl C−H stretches can be attributed to the orientation of the transition dipole moment (TDM) arising from the stretches and the surface selection rules that govern the PM-IRRAS technique.[52] The disorder introduced into the films by the headgroup architecture and the quaternary ammonium groups can plausibly cause the methyl moieties to adopt an orientation in which the TDM lies parallel to the metal surface, leading to a peak that is not detectable. It is also worth noting that the $\nu_a^{CH_2}$ peak positions of the SAMs derived from the bidentate adsorbates **C15-DT**, **TEA-C15-DT**, and **TMA-C15-DT** were very similar (~2926 cm^{-1}) to each other and are higher than the position of the $\nu_a^{CH_2}$ peaks of the monodentate SAMs. This observation can be rationalized by the lower packing density of the bidentate

DOI: 10.1021/acsami.8b12244
ACS Appl. Mater. Interfaces 2018, 10, 40890−40900

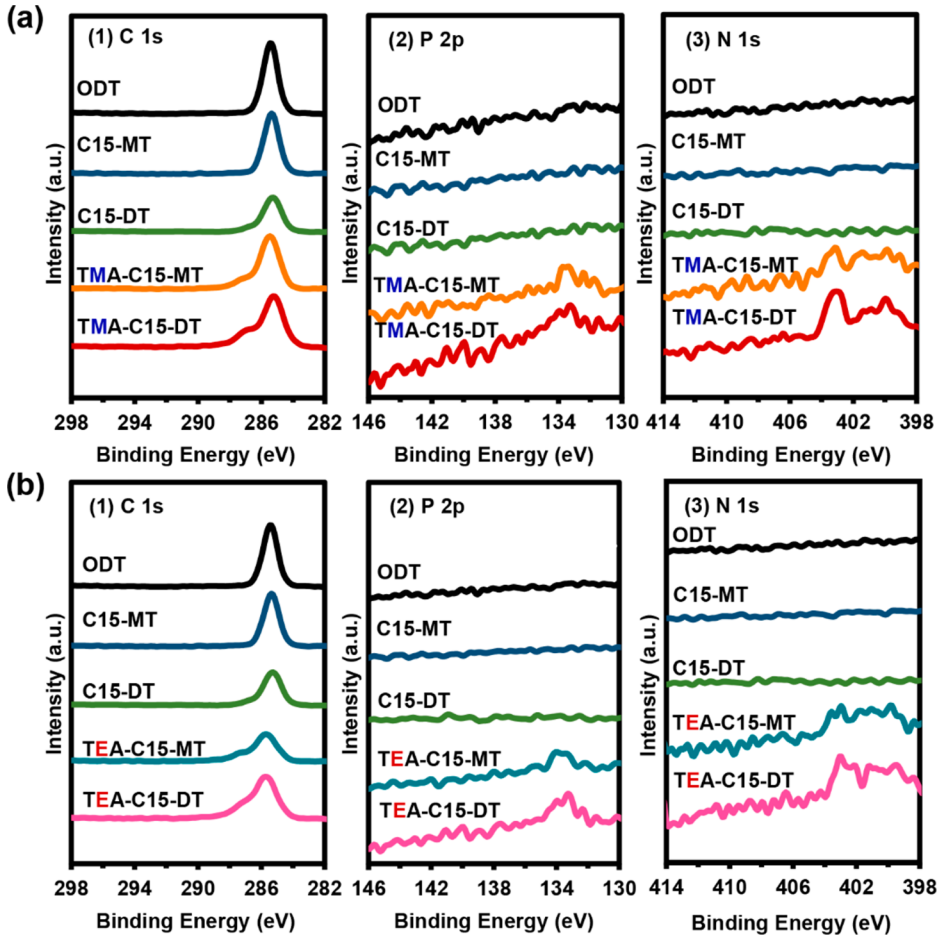

Figure 4. XPS spectra for the (A) trimethylammonium-terminated SAMs (**TMA-C15-MT** and **TMA-C15-DT**) and (B) triethylammonium-terminated SAMs (**TEA-C15-MT** and **TEA-C15-DT**) for the (1) C 1s, (2) P 2p, and (3) N 1s regions. The SAMs generated from the methyl-terminated adsorbates (**ODT**, **C15-MT**, and **C15-DT**) are included in both panels for comparison.

adsorbates compared to the monodentate ammonium-terminated adsorbates. Overall, the PM-IRRAS data indicate that the conformational order of the films decreases as follows: **ODT** = **C15-MT** > **TMA-C15-MT** > **TEA-C15-MT** > **C15-DT** = **TMA-C15-DT** > **TEA-C15-DT**.

Quartz Crystal Microbalance Studies of SAM Formation. To measure the amount of adsorbate chemisorbed onto the substrate, electrochemical quartz crystal microbalance (eQCM) was used. The change in frequency (Hz) was measured, and the mass (μg) was calculated using the Sauerbrey equation (eq 1)[53,54]

$$\Delta f = -C_f \times \Delta m \quad (1)$$

In this equation, Δf denotes the change in the frequency of the formed adsorbate minus the initial frequency collected from the bare QCM without the SAM. The term C_f represents the sensitivity of the crystal, 226 μg/cm^2, which is provided by the manufacturer. The changes in the frequencies of the **TMA-C15-MT**, **TEA-C15-MT**, **TMA-C15-DT**, and **TEA-C15-DT** SAMs are presented in Figure S7a, and the calculated masses derived from the Sauerbrey equation are presented in Figure S7b. The masses calculated from the data suggest that **TMA-C15-MT** has the largest mass per unit area (0.47 μg/cm^2) among the quaternary ammonium-terminated SAMs. Furthermore, for the monodentate adsorbates, the adsorbate with the larger tailgroup, **TEA-C15-MT**, showed a lower value than did **TMA-C15-MT** (0.44 vs 0.47 μg/cm^2). Comparatively, the calculated masses obtained from the bidentate **TEA-C15-DT** and **TMA-C15-DT** SAMs (0.38 vs 0.43 μg/cm^2, respectively) show a similar trend. Overall, with regard to the amount of adsorbate present on the surface, the analysis indicates the following trend: **TMA-C15-MT** > **TEA-C15-MT** > **TMA-C15-DT** > **TEA-C15-DT**, which is consistent with the XPS results (vide supra). Overall, the amount of adsorbate determined from the eQCM data, the packing density analysis, and the conformational order of the films suggest that both the quaternary ammonium terminal group and the adsorbate headgroup influence the structural properties of the films.

Immobilization of Oligonucleotides on Single-Component SAMs. *Immobilization of Oligonucleotides: Analysis of Film Thickness.* The thickness measurements of the films before and after the conjugation of the oligonucleotides are presented in Table S2. The changes in film thickness determined by ellipsometry were used as a guide to determine whether the oligonucleotide bound to the surface. For the methyl-terminated SAMs, **ODT**, **C15-MT**, and **C15-DT**, there was no change in the thickness upon incubation with the oligonucleotide, as expected for hydrocarbon-terminated surfaces. On the other hand, the SAMs derived from the quaternary ammonium-terminated adsorbates **TMA-C15-MT**, **TEA-C15-MT**, **TMA-C15-DT**, and **TEA-C15-DT** each exhibited a 4 Å increase in thicknesses upon conjugation

DOI: 10.1021/acsami.8b12244
ACS Appl. Mater. Interfaces 2018, 10, 40890−40900

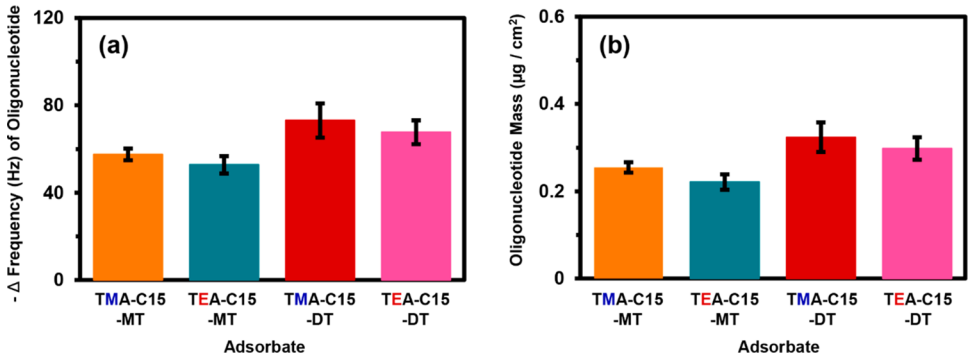

Figure 5. Oligonucleotide loading after immobilization onto the quaternary ammonium-terminated SAMs. (a) Change in frequency on a 10 MHz quartz crystal, and (b) calculated mass per unit area of immobilized oligonucleotides onto SAMs derived from **TMA-C15-MT**, **TEA-C15-MT**, **TMA-C15-DT**, and **TEA-C15-DT**.

with the oligonucleotide. This increase in thickness can be attributed to electrostatic interactions between the quaternary ammonium group and the phosphate backbone of the oligonucleotide.[23,55] Based on this result and the packing density analysis above, we propose that the increase in thickness is due to the intercalation of the oligonucleotides into the cavities formed by the bulky charged adsorbates.[27]

Immobilization of Oligonucleotides: Analysis by XPS. To probe for the presence of the oligonucleotides, the SAMs were examined for peaks characteristic of the phosphate backbone and the nitrogenous bases. The XPS spectra for the P 2p, C 1s, and N 1s regions for the SAMs after the immobilization of the oligonucleotides are presented in Figure 4. The P $2p_{3/2}$ photoelectron of the phosphate backbone has been reported as having a binding energy of ~133 eV.[56,57] Furthermore, the nitrogen atoms in nitrogenous bases exhibit a characteristic N 1s peak at ~400 eV, while the C−N carbon in the C 1s region is located at ~286 eV (Figures 4a1,b1).[58]

Notably, the methyl-terminated SAMs derived from **ODT**, **C15-MT**, and **C15-DT** exhibited no peaks characteristic of the oligonucleotides in their XPS spectra, which is consistent with the ellipsometry studies and with the inability of the oligonucleotides to interact electrostatically with the terminal group of these SAMs. In contrast, the SAMs derived from **TMA-C15-MT**, **TEA-C15-MT**, **TMA-C15-DT**, and **TEA-C15-DT** showed phosphorus originating from the oligonucleotide phosphate backbone at ~133 eV (Figures 4a2,a2). Furthermore, the presence of the amide heterocycles (purine and pyrimidine) in the oligonucleotides was confirmed by the appearance of a new peak at ~400 eV in the N 1s region (Figures 4a3,b3). Overall, the XPS studies argue that oligonucleotide immobilization was successfully achieved due to electrostatic interactions between the phosphate backbone and the charged terminal groups of the ammonium-terminated SAMs, consistent with the ellipsometry results.

Immobilization of Oligonucleotides: Analysis by Quartz Crystal Microbalance. Information obtained from QCM offers valuable insight into the loading capability of the SAMs derived from the monothiols (**TMA-C15-MT** and **TEA-C15-MT**) and the dithiols (**TMA-C15-DT** and **TEA-C15-DT**). The oligonucleotide masses on the SAM surfaces (see Figure 5a) were calculated from the QCM measurements, which were determined from the difference in the frequency of the samples prior to and after immobilization of the oligonucleotides using the Sauerbrey equation. The oligonucleotide masses per unit area for the monodenatate SAMs derived from **TMA-C15-MT** and **TEA-C15-MT** were found to be 0.25 and 0.22 $\mu g/cm^2$, respectively, while those for the bidentate SAMs derived from **TMA-C15-DT** and **TEA-C15-DT** were found to be 0.32 and 0.30 $\mu g/cm^2$, respectively (see Figure 5b). The greater mass loading for the bidentate SAMs compared to the monodentate SAMs can plausibly arise from the loose packing densities of the bidentate films, which facilitates oligonucleotide intercalation into these SAMs. In this respect, SAMs derived from **TMA-C15-DT** showed the greatest mass loading per cm^2 when compared to all other single-component surfaces studied. Based on this data set, we inferred that the ideal surface needed to maximize oligonucleotide immobilization should have a bidentate headgroup architecture and a relatively small positively charged tailgroup. To create such surfaces, we explored the use of mixed adsorbate systems (vide infra).

Mixed SAMs Derived from Selected Ratios of TMA-C15-DT and TMA-C6-DT. In efforts to maximize the immobilization of oligonucleotides on the SAMs, we designed and synthesized a shorter alkyl chain derivative of **TMA-C15-DT**, **TMA-C6-DT**, to use in the formation of mixed SAMs. Binary mixed SAMs containing a mixture of short and long alkyl chain adsorbates have been shown to exhibit the following features and abilities: (1) diminished packing densities compared to single-adsorbate films, (2) diminished steric hindrance between terminal groups during the immobilization of biomolecules,[59] and (3) enhanced immobilization of oligonucleotides.[59,60] We formed mixed SAMs on gold using systematically selected ratios of **TMA-C15-DT** and **TMA-C6-DT**. We set forth to determine: (1) the correlation between the amount of **TMA-C6-DT** and **TMA-C15-DT** and the packing density of the film, and (2) the ideal concentrations of **TMA-C15-DT** and **TMA-C6-DT** to immobilize the maximum possible amount of oligonucleotides onto these surfaces. The mixed SAM surfaces were analyzed using the techniques of ellipsometry, XPS, eQCM, and PM-IRRAS both prior to and after immobilization of the oligonucleotides.

Mixed Bidentate SAMs: Measurements of Film Thickness. The ellipsometry data for the SAMs generated from mixtures of **TMA-C15-DT** and **TMA-C6-DT** are given in Table 2. For clarity, the mole fraction of the adsorbate in solution for each of the mixed SAMs is denoted in parentheses. Monolayers generated from **TMA-C15-DT** (1.0), **TMA-C15-DT** (0.75), **TMA-C15-DT** (0.50), **TMA-C15-DT** (0.25), and **TMA-C6-DT** (1.0) have film thicknesses of 22, 20, 18, 16, and 15 Å, respectively. The data in Table 2 show a systematic decrease in

DOI: 10.1021/acsami.8b12244
ACS Appl. Mater. Interfaces 2018, 10, 40890−40900

Table 2. Ellipsometric Thicknesses, Relative Packing Densities, and Bound Sulfur Contents of Mixed SAMs Formed Using Systematically Varying Ratios of Adsorbates

adsorbate	ellipsometric film thickness (Å)	relative packing density (%)	percentage of bound sulfur (%)
ODT	23 ± 1	100	100
TMA-C15-DT (1.0)	22 ± 1	47 ± 2	82 ± 4
TMA-C15-DT (0.75)	20 ± 1	38 ± 3	76 ± 1
TMA-C15-DT (0.50)	18 ± 1	36 ± 1	66 ± 1
TMA-C15-DT (0.25)	16 ± 1	35 ± 2	60 ± 2
TMA-C6-DT (1.0)	15 ± 1	32 ± 1	58 ± 3

the film thickness as the content of **TMA-C6-DT** increases, which is consistent with the shortening of the length of the alkyl spacer (i.e., from 15 CH_2 groups for **TMA-C15-DT** to 6 CH_2 groups for **TMA-C6-DT**). In the mixed SAMs with greater amounts of **TMA-C6-DT**, it is plausible that the lower portion of the films is densely packed, leaving the **TMA-C15-DT** in the top portion of the film to be loosely packed and disordered, with a more fluidlike structure.[38]

Mixed Bidentate SAMs: Analysis by XPS. The chemical compositions of the mixed SAMs are depicted in Figure 6, which shows the XPS spectra for the Br 3d, S 2p, C 1s, and N 1s regions. Separately, the binding energy region of the Au $4f_{7/2}$ electrons, which are used as a reference for calibrating the XPS signal intensities, is shown in Figure S8. All samples tested, with the exception of **ODT**, showed characteristic peaks for the Br $3d_{3/2}$ and Br $3d_{5/2}$ photoelectrons at binding energies of ~68 and ~67 eV, respectively, and N 1s electrons characteristic of the trialkyammonium group at ~403 eV.[27] As the amount of **TMA-C15-DT** was systematically decreased in the mixture, there was a corresponding reduction in the intensity of the Br 3d peaks and an increase in intensity for a new peak at ~197 eV for Cl 2p, in accordance with the systematic introduction of **TMA-C6-DT**, whose counterion was Cl (see Figure S9). As illustrated by Figure S9, the detection of chloride ions by XPS at low concentrations in SAMs is challenging.[61]

The incorporation of the shorter **TMA-C6-DT** adsorbate into the mixed SAM can also be gleaned from the gradual decrease in intensity of the methylene carbons in the C 1s region. The methylene spacer for **TMA-C6-DT**, being shorter than that for **TMA-C15-DT**, is responsible for the gradual decrease. Analysis of the S 2p region, including the deconvolution of the S 2p peaks (see Figure S10), can be used to determine the amounts of bound and unbound thiol in the mixed SAMs, which are given in Table 2 and are consistent with the results obtained from the studies of the single-component monolayers.[7,9,41,42] Furthermore, the relative packing densities for the mixed SAMs can be determined as described above and are reported in Table 2. The packing densities decrease in the following order: **ODT** > **TMA-C15-DT** (1.0) > **TMA-C15-DT** (0.75) > **TMA-C15-DT** (0.50) > **TMA-C15-DT** (0.25) > **TMA-C6-DT** (1.0), where the trend is consistent with decreasing interchain van der Waals (vdW) interactions within the film as **TMA-C15-DT** is replaced by **TMA-C6-DT**.

Mixed Bidentate SAMs: Analysis by PM-IRRAS. To evaluate the conformational order of the mixed SAMs, all surfaces were analyzed with PM-IRRAS. The PM-IRRAS spectra obtained in the C−H stretching region are shown in Figure S11. Apparent from the progressive shift of the $\nu_a^{CH_2}$ peak of the mixed SAMs to higher wavenumbers as the amount of **TMA-C6-DT** was increased, the introduction of **TMA-C6-DT** into the **TMA-C15-DT** SAM leads to a decrease in the conformational order of the alkyl chains in the films. The introduction of the shorter alkyl chains of **TMA-C6-DT** plausibly disrupts the stabilizing interchain van der Waals (vdW) interactions within the film derived from **TMA-C15-DT**.

Mixed Bidentate SAMs: Mass Loading Analysis by eQCM. To evaluate further the chemisorption of the mixed SAM adsorbates onto the surface of gold, eQCM was used to monitor the adsorption process. The change in frequency and the mass per unit area of the crystals, derived from the Sauerbrey equation, are presented in Figure 7. The decrease observed in the frequency of the eQCM analysis as **TMA-C6-DT** is introduced into the film reflects an overall decrease in the adsorbate mass, which is consistent with the smaller mass of **TMA-C6-DT** compared to that of **TMA-C15-DT**. Specifically, the amount of adsorbate per unit area for **TMA-C15-DT** (1.0), **TMA-C15-DT** (0.75), **TMA-C15-DT** (0.50),

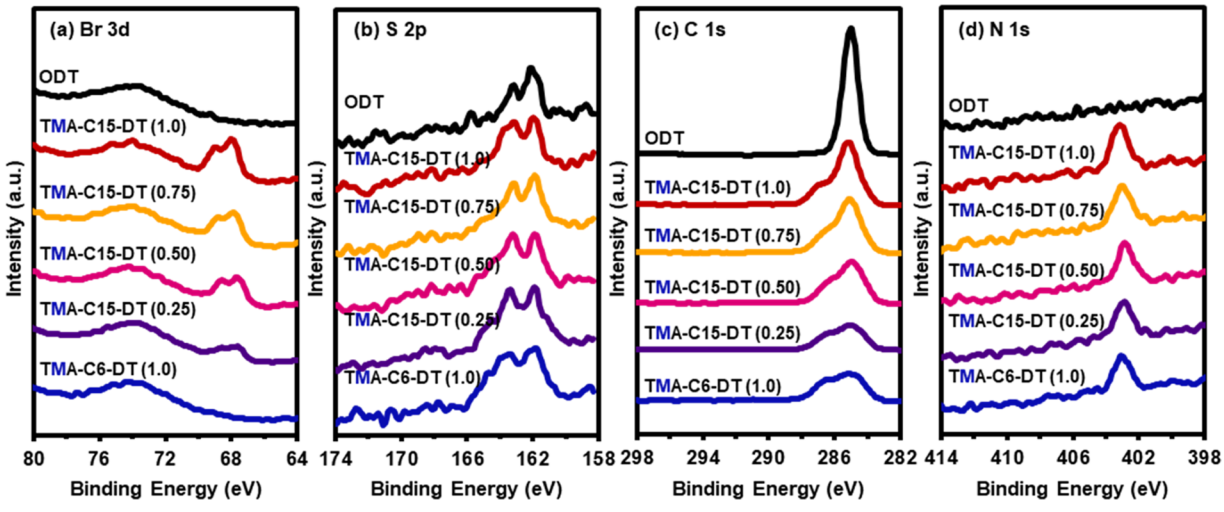

Figure 6. XPS spectra of the mixed SAMs composed of various ratios of **TMA-C15-DT** and **TMA-C6-DT** in the (a) Br 3d, (b) S 2p, (c) C 1s, and (d) N 1s regions. SAMs generated from **ODT** are included as a reference.

DOI: 10.1021/acsami.8b12244
ACS Appl. Mater. Interfaces 2018, 10, 40890−40900

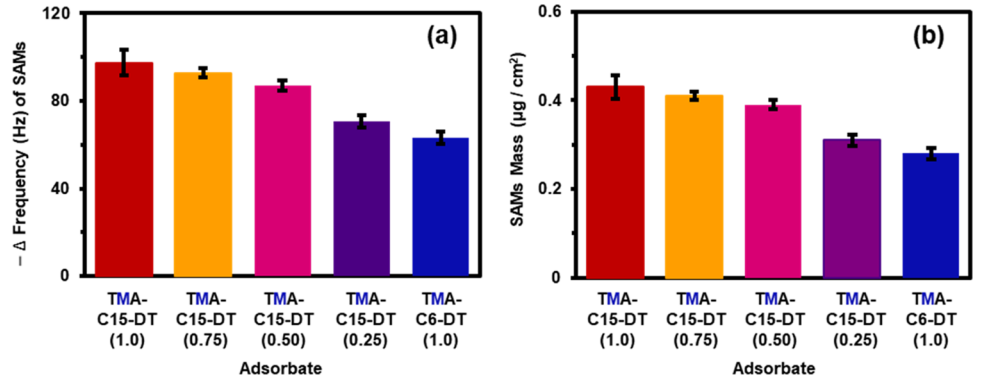

Figure 7. (a) Change in frequency on a 10 MHz eQCM crystal after formation of the mixed SAMs, and (b) mass of the adsorbates per unit area for mixed SAMs derived from various mixtures of **TMA-C15-DT** and **TMA-C6-DT**.

TMA-C15-DT (0.25), and **TMA-C6-DT** (1.0) indicates a decreasing adsorbate mass as the ratio of **TMA-C6-DT** is increased, with mass loading values of 0.43, 0.41, 3.9, 0.31, and 0.28 $\mu g/cm^2$ for **TMA-C15-DT** (1.0), **TMA-C15-DT** (0.75), **TMA-C15-DT** (0.50), **TMA-C15-DT** (0.25), and **TMA-C6-DT** (1.0), respectively. Importantly, the values for the mixed SAMs fall between those of the homologous SAMs, which is consistent with a mixture of the two adsorbates.

Immobilization of Oligonucleotides on SAMs Derived from Mixtures of TMA-C15-DT and TMA-C6-DT. *Analysis of Film Thickness.* Before and after the immobilization of the oligonucleotides, the film thicknesses for the SAMs derived from **TMA-C15-DT** (1.0), **TMA-C15-DT** (0.75), **TMA-C15-DT** (0.50), **TMA-C15-DT** (0.25), and **TMA-C6-DT** (1.0) were measured and are reported in Table 3. The corresponding

Table 3. Ellipsometric Thicknesses of Mixed SAMs Formed Using Various Ratios of Adsorbates Prior to and after the Addition of Oligonucleotides

adsorbate	before conjugation (Å)	after conjugation (Å)	difference (Å)
ODT	23 ± 1	–	–
TMA-C15-DT (1.0)	22 ± 1	26 ± 1	4
TMA-C15-DT (0.75)	20 ± 1	25 ± 1	5
TMA-C15-DT (0.50)	18 ± 1	26 ± 1	8
TMA-C15-DT (0.25)	16 ± 1	22 ± 1	6
TMA-C6-DT (1.0)	15 ± 1	17 ± 1	2

differences in film thickness after conjugation were 4, 5, 8, 6, and 2 Å, respectively (see Table 3). Based on the data obtained, the **TMA-C15-DT** (0.50) surface displayed the most ideal packing density to allow maximum amount of intercalation of oligonucleotides into the interior of the SAMs. Apparent from the data, there is a delicate balance between chain length and packing density/order in constructing the ideal surface. On the densely packed, conformationally ordered **TMA-C15-DT** SAMs, there is no void space to accommodate the intercalating oligonucleotides. Similarly, for the short (thin) **TMA-C6-DT** SAMs, there is little or no void space to accommodate the intercalating oligonucleotides. In contrast, the mixed SAMs (and particularly for **TMA-C15-DT** (0.50), where the mixture is roughly 50:50) offer loose packing and void space to accommodate the intercalating oligonucleotides.

Immobilization of Oligonucleotides on Mixed Bidentate SAMs: Analysis by XPS. The SAMs were analyzed by XPS after the immobilization of the oligonucleotides to evaluate immobilization by focusing the analysis in the P 2p, C 1s, and N 1s regions (Figure 8). After the incubation of the oligonucleotides with the SAMs, the presence of a peak in the P 2p region (Figure 8a) at ~133 eV was found in all quaternary ammonium-terminated SAMs. Specifically, the phosphorous photoelectrons originate from the phosphate backbone of the oligonucleotides, which joins the 3′ and 5′ carbon of the nucleotides via a phosphodiester bond.[62] The charged phosphate backbone allows for an electrostatic interaction between the quaternary ammonium termini of the SAMs and the oligonucleotides. The C−N carbons of the nitrogenous bases were also found at ~286 eV; correspondingly, analysis of the N 1s region (Figure 8c) also confirms the presence of the nitrogenous bases with a broad peak at ~400 eV corresponding to the heterocyclic structure (purine and pyrimidine) found in the nucleic acid sequence.[58,61] Further analysis of the C 1s region (Figure 8b) confirms the presence of the SAM architecture with the methylene carbons at ~285 eV and the C−O carbon at 286.6 eV.[27,43,44]

Immobilization of Oligonucleotides on Mixed Bidentate SAMs: Mass Loading Analysis by eQCM. The relationship between the packing density of the mixed **TMA-C15-DT** and **TMA-C6-DT** SAMs and the immobilization of the oligonucleotide was explored by calculating the mass of oligonucleotide on the surface using eQCM. The change in frequency of the SAMs after immobilization with the oligonucleotides, shown in Figure 9a, was used to obtain the mass of the oligonucleotides by using the Sauerbrey equation. The mass values obtained for the SAMs derived from **TMA-C15-DT** (1.0), **TMA-C15-DT** (0.75), **TMA-C15-DT** (0.50), **TMA-C15-DT** (0.25), and **TMA-C6-DT** (1.0) are shown in Figure 9b and are as follows: 0.32, 1.44, 2.15, 1.14, and 0.39 $\mu g/cm^2$, respectively. Based on the mass loading analysis, the 50:50 mixture of **TMA-C15-DT** and **TMA-C6-DT** gave the maximum number of conjugated oligonucleotides. The overall loading of oligonucleotides determined from the eQCM data decreases as follows: **TMA-C15-DT** (0.50) > **TMA-C15-DT** (0.75) > **TMA-C15-DT** (1.0) > **TMA-C15-DT** (0.25) > **TMA-C6-DT** (1.0). Based on these results, the heterogeneous SAMs, particularly those derived from a 50:50 molar fraction ratio of **TMA-C15-DT** to **TMA-C6-DT**, appear to bind the greatest amount of oligonucleotides on their surfaces. As noted above, these mixed SAMs offer the most loosely packed chains and the greatest void space to accommodate the intercalating oligonucleotides.

DOI: 10.1021/acsami.8b12244
ACS Appl. Mater. Interfaces 2018, 10, 40890−40900

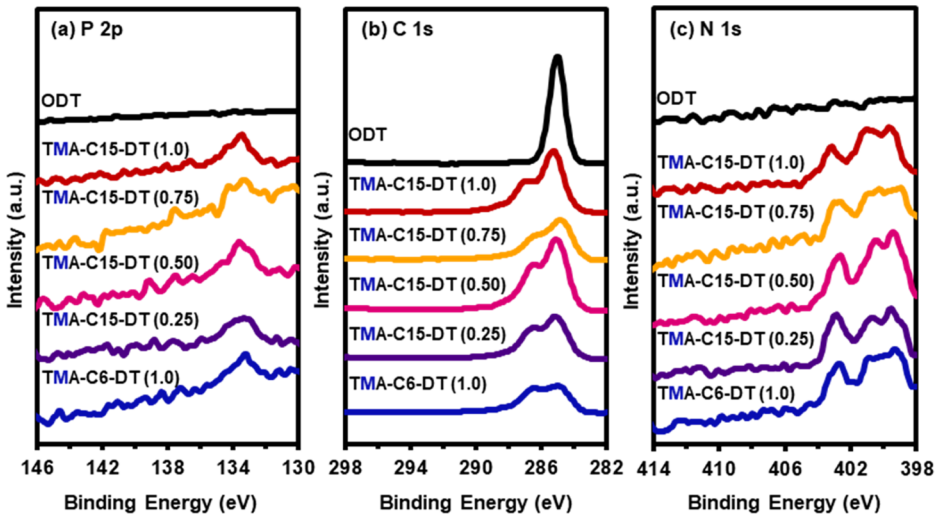

Figure 8. XPS spectra of the mixed SAMs composed of various ratios of **TMA-C15-DT** and **TMA-C6-DT** in the (a) P 2p, (b) C 1s, and (c) N 1s regions. SAMs generated from **ODT** are included as a reference.

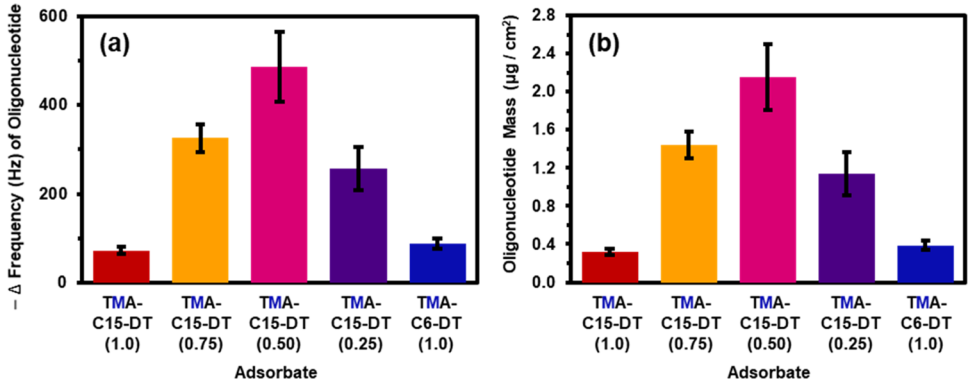

Figure 9. (a) Change in frequency on a 10 MHz eQCM crystal after immobilization with oligonucleotides. (b) Calculated mass per unit area of immobilized oligonucleotides onto mixed SAMs derived from selected mixtures of **TMA-C15-DT** and **TMA-C6-DT**.

CONCLUSIONS

Six unique thiol-based adsorbates, each possessing a quaternary ammonium terminal group, were successfully synthesized and used to generate SAMs on gold for the immobilization of oligonucleotides. The chemical composition of the SAMs was evaluated by XPS, revealing a diminished tailgroup packing density for the quaternary ammonium-terminated SAMs when compared to their methyl-terminated analogs. The immobilization of the oligonucleotides was verified by XPS and quantified with eQCM. The detection of phosphorus from the phosphate backbone of the oligonucleotides as well as the carbon and nitrogen from the nucleic acids confirmed the presence of the immobilized oligonucleotides. Furthermore, the headgroup architecture and the size of the quaternary ammonium group of the adsorbate were found to influence the loading capability of the SAMs. The diminished packing densities afforded by the bulky bidentate headgroup of the quaternary ammonium-terminated SAMs allow for the intercalation of the oligonucleotide into the interspace of the SAMs. To maximize the amount of oligonucleotides immobilized onto these types of surfaces, mixed SAMs composed of various ratios of long-chain **TMA-C15-DT** and a shorter analog, **TMA-C6-DT**, were used to generate films with loosely packed tailgroups (and thus maximum void space for oligonucleotide immobilization). Our studies found that a 50:50 mixture of **TMA-C15-DT** and **TMA-C6-DT** formed the ideal surface for an approximately 10-fold increase in the loading capability of these types of surfaces (i.e., 0.25 $\mu g/cm^2$ for the single-component SAM derived from **TMA-C15-DT** vs 2.15 $\mu g/cm^2$ for the mixed SAM). The ideal conditions outlined above for maximum oligonucleotide immobilization open new avenues for future studies and therapeutic applications involving SAMs derived from 50:50 mixtures of **TMA-C15-DT** and **TMA-C6-DT** on gold nanoparticles and nanoshells for oligonucleotide delivery.

EXPERIMENTAL SECTION

A detailed description regarding the materials, methods, instrumentation, and synthetic procedures is provided in the Supporting Information. Comprehensive characterization of the adsorbates [(**TMA-C15-MT**, **TEA-C15-MT**, **C15-DT**, **TMA-C15-DT**, **TMA-C6-DT**, and **TEA-C15-DT**)] using ^{1}H NMR spectroscopy, ^{13}C NMR spectroscopy, and liquid chromatography−mass spectrometry is presented in the Supporting Information (Figures S12−S23).

ASSOCIATED CONTENT

Supporting Information

The Supporting Information is available free of charge on the ACS Publications website at DOI: 10.1021/acsami.8b12244.

DOI: 10.1021/acsami.8b12244
ACS Appl. Mater. Interfaces 2018, 10, 40890−40900

Additional XPS spectra, experimental parameters, eQCM, comprehensive synthetic procedures, and characterization (^{1}H and ^{13}C NMR spectra) for all molecules (**TMA-C15-MT**, **TEA-C15-MT**, **C15-DT**, **TMA-C6-DT**, **TMA-C15-DT**, and **TEA-C15-DT**) can be obtained (PDF)

AUTHOR INFORMATION

Corresponding Authors

*E-mail: phgunaratne@uh.edu (P.H.G.).
*E-mail: trlee@uh.edu (T.R.L.).

ORCID

T. Randall Lee: 0000-0001-9584-8861

Notes

The authors declare no competing financial interest.

ACKNOWLEDGMENTS

We thank the National Science Foundation (CHE-1710561, T.R.L.), the Robert A. Welch Foundation (grant no. E-1320, T.R.L.), the Cancer Prevention and Research Institute of Texas (RP110355; P.H.G.), and the Texas Center for Superconductivity at the University of Houston (T.R.L.) for generous financial support.

REFERENCES

(1) Holmlin, R. E.; Chen, X.; Chapman, R. G.; Takayama, S.; Whitesides, G. M. Zwitterionic SAMs that Resist Nonspecific Adsorption of Protein from Aqueous Buffer. *Langmuir* **2001**, *17*, 2841−2850.

(2) Li, B.; Ye, Q. Antifouling Surfaces of Self-assembled Thin Layer. In *Antifouling Surfaces and Materials: From Land to Marine Environment*; Zhou, F., Ed.; Springer: Berlin, Heidelberg, 2015; pp 31−54.

(3) Huang, C.-J.; Chang, Y.-C. In Situ Surface Tailoring with Zwitterionic Carboxybetaine Moieties on Self-Assembled Thin Film for Antifouling Biointerfaces. *Materials* **2014**, *7*, 130−142.

(4) Smet, L. C. P. M. D.; Ullien, D.; Mescher, M.; Sudhölter, E. J. R. Organic Surface Modification of Silicon Nanowire-Based Sensor Devices. In *Nanowires: Implementations and Applications*; Hashim, A., Ed.; InTech: Rijeka, 2011; p 13.

(5) Banga, R. J.; Krovi, S. A.; Narayan, S. P.; Sprangers, A. J.; Liu, G.; Mirkin, C. A.; Nguyen, S. T. Drug-Loaded Polymeric Spherical Nucleic Acids: Enhancing Colloidal Stability and Cellular Uptake of Polymeric Nanoparticles through DNA Surface-Functionalization. *Biomacromolecules* **2017**, *18*, 483−489.

(6) Charles, P. T.; Vora, G. J.; Andreadis, J. D.; Fortney, A. J.; Meador, C. E.; Dulcey, C. S.; Stenger, D. A. Fabrication and Surface Characterization of DNA Microarrays Using Amine- and Thiol-Terminated Oligonucleotide Probes. *Langmuir* **2003**, *19*, 1586−1591.

(7) Vericat, C.; Vela, M. E.; Corthey, G.; Pensa, E.; Cortes, E.; Fonticelli, M. H.; Ibanez, F.; Benitez, G. E.; Carro, P.; Salvarezza, R. C. Self-Assembled Monolayers of Thiolates on Metals: a Review Article on Sulfur-Metal Chemistry and Surface Structures. *RSC Adv.* **2014**, *4*, 27730−27754.

(8) Love, J. C.; Estroff, L. A.; Kriebel, J. K.; Nuzzo, R. G.; Whitesides, G. M. Self-Assembled Monolayers of Thiolates on Metals as a Form of Nanotechnology. *Chem. Rev.* **2005**, *105*, 1103−1170.

(9) Lee, H. J.; Jamison, A. C.; Lee, T. R. Boc-Protected ω-Amino Alkanedithiols Provide Chemically and Thermally Stable Amine-Terminated Monolayers on Gold. *Langmuir* **2015**, *31*, 2136−2146.

(10) Chechik, V.; Stirling, C. J. M. Reactivity in Self-Assembled Monolayers: Effect of the Distance from the Reaction Center to the Monolayer−Solution Interface. *Langmuir* **1998**, *14*, 99−105.

(11) Techane, S. D.; Gamble, L. J.; Castner, D. G. Multitechnique Characterization of Self-Assembled Carboxylic Acid-Terminated Alkanethiol Monolayers on Nanoparticle and Flat Gold Surfaces. *J. Phys. Chem. C* **2011**, *115*, 9432−9441.

(12) Jadhav, S. A. Self-Assembled Monolayers (SAMs) of Carboxylic Acids: an Overview. *Cent. Eur. J. Chem.* **2011**, *9*, 369−378.

(13) Samanta, D.; Sarkar, A. Immobilization of Bio-Macromolecules on Self-Assembled Monolayers: Methods and Sensor Applications. *Chem. Soc. Rev.* **2011**, *40*, 2567−2592.

(14) Chen, Y.; Nguyen, A.; Niu, L.; Corn, R. M. Fabrication of DNA Microarrays with Poly(l-glutamic acid) Monolayers on Gold Substrates for SPR Imaging Measurements. *Langmuir* **2009**, *25*, 5054−5060.

(15) Smith, E. A.; Wanat, M. J.; Cheng, Y.; Barreira, S. V. P.; Frutos, A. G.; Corn, R. M. Formation, Spectroscopic Characterization, and Application of Sulfhydryl-Terminated Alkanethiol Monolayers for the Chemical Attachment of DNA onto Gold Surfaces. *Langmuir* **2001**, *17*, 2502−2507.

(16) Brockman, J. M.; Frutos, A. G.; Corn, R. M. A Multistep Chemical Modification Procedure To Create DNA Arrays on Gold Surfaces for the Study of Protein−DNA Interactions with Surface Plasmon Resonance Imaging. *J. Am. Chem. Soc.* **1999**, *121*, 8044−8051.

(17) Lee, M.-Y.; Park, S.-J.; Park, K.; Kim, K. S.; Lee, H.; Hahn, S. K. Target-Specific Gene Silencing of Layer-by-Layer Assembled Gold−Cysteamine/siRNA/PEI/HA Nanocomplex. *ACS Nano* **2011**, *5*, 6138−6147.

(18) Rianasari, I.; Walder, L.; Burchardt, M.; Zawisza, I.; Wittstock, G. Inkjet-Printed Thiol Self-Assembled Monolayer Structures on Gold: Quality Control and Microarray Electrode Fabrication. *Langmuir* **2008**, *24*, 9110−9117.

(19) Jang, L.-S.; Keng, H.-K. Modified Fabrication Process of Protein Chips Using a Short-Chain Self-Assembled Monolayer. *Biomed. Microdevices* **2008**, *10*, 203−211.

(20) Takeo, M.; Takashi, T.; Koichi, K.; Tamotsu, Z.; Takashi, F.; Iwao, O. Selectivity Improvement in Protein Nanopatterning with a Hydroxy-Terminated Self-Assembled Monolayer Template. *Nanotechnology* **2007**, *18*, No. 305304.

(21) Basabe-Desmonts, L.; van der Baan, F.; Zimmerman, R. S.; Reinhoudt, D. N.; Crego-Calama, M. Cross-Reactive Sensor Array for Metal Ion Sensing Based on Fluorescent SAMs. *Sensors* **2007**, *7*, 1731−1746.

(22) Braiek, M.; Rokbani, K. B.; Chrouda, A.; Mrabet, B.; Bakhrouf, A.; Maaref, A.; Jaffrezic-Renault, N. An Electrochemical Immunosensor for Detection of *Staphylococcus aureus* Bacteria Based on Immobilization of Antibodies on Self-Assembled Monolayers-Functionalized Gold Electrode. *Biosensors* **2012**, *2*, 417−426.

(23) Reinhardt, N.; Adumeau, L.; Lambert, O.; Ravaine, S.; Mornet, S. Quaternary Ammonium Groups Exposed at the Surface of Silica Nanoparticles Suitable for DNA Complexation in the Presence of Cationic Lipids. *J. Phys. Chem. B* **2015**, *119*, 6401−6411.

(24) Higashi, N.; Inoue, T.; Niwa, M. Immobilization and Cleavage of DNA at Cationic, Self-Assembled Monolayers Containing C60 on Gold. *Chem. Commun.* **1997**, 1507−1508.

(25) Wang, J.; Lu, Z.; Wientjes, M. G.; Au, J. L. S. Delivery of siRNA Therapeutics: Barriers and Carriers. *AAPS J.* **2010**, *12*, 492−503.

(26) Lee, S.-H.; Lin, W.-C.; Kuo, C.-H.; Karakachian, M.; Lin, Y.-C.; Yu, B.-Y.; Shyue, J.-J. Photooxidation of Amine-Terminated Self-Assembled Monolayers on Gold. *J. Phys. Chem. C* **2010**, *114*, 10512−10519.

(27) Ah Qune, L. F. N.; Makino, K.; Tamada, K.; Chen, W.; Wee, A. T. S. Selective Adsorption of l-Tartaric Acid on Gemini-Type Self-Assembled Monolayers. *J. Phys. Chem. C* **2008**, *112*, 3049−3053.

(28) Yokokawa, S.; Tamada, K.; Ito, E.; Hara, M. Cationic Self-Assembled Monolayers Composed of Gemini-Structured Dithiol on Gold: A New Concept for Molecular Recognition Because of the Distance between Adsorption Sites. *J. Phys. Chem. B* **2003**, *107*, 3544−3551.

(29) Rittikulsittichai, S.; Park, C. S.; Jamison, A. C.; Frank, T.; Wu, C.-H.; Wu, J. I.; Lee, T. R.; et al. Inhibiting Reductive Elimination as an Intramolecular Disulfide Dramatically Enhances the Thermal

DOI: 10.1021/acsami.8b12244
ACS Appl. Mater. Interfaces 2018, 10, 40890−40900

Stability of SAMs on Gold Derived from Bidentate Adsorbates. *Langmuir* **2018**, *34*, 6645−6652.
(30) Ghosh, R.; Singh, L. C.; Shohet, J. M.; Gunaratne, P. H. A Gold Nanoparticle Platform for the Delivery of Functional microRNAs into Cancer Cells. *Biomaterials* **2013**, *34*, 807−816.
(31) Guo, S.; Huang, Y.; Jiang, Q.; Sun, Y.; Deng, L.; Liang, Z.; Du, Q.; Xing, J.; Zhao, Y.; Wang, P. C.; Dong, A.; Liang, X.-J. Enhanced Gene Delivery and siRNA Silencing by Gold Nanoparticles Coated with Charge-Reversal Polyelectrolyte. *ACS Nano* **2010**, *4*, 5505−5511.
(32) Kim, H. J.; Takemoto, H.; Yi, Y.; Zheng, M.; Maeda, Y.; Chaya, H.; Hayashi, K.; Mi, P.; Pittella, F.; Christie, R. J.; Toh, K.; Matsumoto, Y.; Nishiyama, N.; Miyata, K.; Kataoka, K. Precise Engineering of siRNA Delivery Vehicles to Tumors Using Polyion Complexes and Gold Nanoparticles. *ACS Nano* **2014**, *8*, 8979−8991.
(33) Braun, G. B.; Pallaoro, A.; Wu, G.; Missirlis, D.; Zasadzinski, J. A.; Tirrell, M.; Reich, N. O. Laser-Activated Gene Silencing via Gold Nanoshell−siRNA Conjugates. *ACS Nano* **2009**, *3*, 2007−2015.
(34) Huschka, R.; Barhoumi, A.; Liu, Q.; Roth, J. A.; Ji, L.; Halas, N. J. Gene Silencing by Gold Nanoshell-Mediated Delivery and Laser-Triggered Release of Antisense Oligonucleotide and siRNA. *ACS Nano* **2012**, *6*, 7681−7691.
(35) Riley, R. S.; Dang, M. N.; Billingsley, M. M.; Abraham, B.; Gundlach, L.; Day, E. S. Evaluating the Mechanisms of Light-Triggered siRNA Release from Nanoshells for Temporal Control Over Gene Regulation. *Nano Lett.* **2018**, *18*, 3565−3570.
(36) Singhana, B.; Slattery, P.; Chen, A.; Wallace, M.; Melancon, M. P. Light-Activatable Gold Nanoshells for Drug Delivery Applications. *AAPS PharmSciTech* **2014**, *15*, 741−752.
(37) Vericat, C.; Vela, M. E.; Benitez, G.; Carro, P.; Salvarezza, R. C. Self-Assembled Monolayers of Thiols and Dithiols on Gold: New Challenges for a Well-Known System. *Chem. Soc. Rev.* **2010**, *39*, 1805−1834.
(38) Bain, C. D.; Whitesides, G. M. Modeling Organic Surfaces with Self-Assembled Monolayers. *Adv. Mater.* **1989**, *1*, 110−116.
(39) Lee, H. J.; Jamison, A. C.; Lee, T. R. Two Are Better than One: Bidentate Adsorbates Offer Precise Control of Interfacial Composition and Properties. *Chem. Mater.* **2016**, *28*, 5356−5364.
(40) Baio, J. E.; Weidner, T.; Brison, J.; Graham, D. J.; Gamble, L. J.; Castner, D. G. Amine Terminated SAMs: Investigating Why Oxygen is Present in These Films. *J. Electron Spectrosc. Relat. Phenom.* **2009**, *172*, 2−8.
(41) Lee, H. J.; Jamison, A. C.; Yuan, Y.; Li, C.-H.; Rittikulsittichai, S.; Rusakova, I.; Lee, T. R. Robust Carboxylic Acid-Terminated Organic Thin Films and Nanoparticle Protectants Generated from Bidentate Alkanethiols. *Langmuir* **2013**, *29*, 10432−10439.
(42) Castner, D. G.; Hinds, K.; Grainger, D. W. X-ray Photoelectron Spectroscopy Sulfur 2p Study of Organic Thiol and Disulfide Binding Interactions with Gold Surfaces. *Langmuir* **1996**, *12*, 5083−5086.
(43) Montague, M.; Ducker, R. E.; Chong, K. S. L.; Manning, R. J.; Rutten, F. J. M.; Davies, M. C.; Leggett, G. J. Fabrication of Biomolecular Nanostructures by Scanning Near-Field Photolithography of Oligo(ethylene glycol)-Terminated Self-Assembled Monolayers. *Langmuir* **2007**, *23*, 7328−7337.
(44) Park, C. S.; Lee, H. J.; Jamison, A. C.; Lee, T. R. Robust Maleimide-Functionalized Gold Surfaces and Nanoparticles Generated Using Custom-Designed Bidentate Adsorbates. *Langmuir* **2016**, *32*, 7306−7315.
(45) Ulman, A. Formation and Structure of Self-Assembled Monolayers. *Chem. Rev.* **1996**, *96*, 1533−1554.
(46) Häkkinen, H. The Gold−Sulfur Interface at the Nanoscale. *Nat. Chem.* **2012**, *4*, 443−455.
(47) Yuan, Y.; Lee, T. R. Contact Angle and Wetting Properties. In *Surface Science Techniques*; Bracco, G., Holst, B., Eds.; Springer: Berlin, Heidelberg, 2013; pp 3−34.
(48) Lee, S.; Puck, A.; Graupe, M.; Colorado, R.; Shon, Y.-S.; Lee, T. R.; Perry, S. S. Structure, Wettability, and Frictional Properties of Phenyl-Terminated Self-Assembled Monolayers on Gold. *Langmuir* **2001**, *17*, 7364−7370.
(49) Bain, C. D.; Troughton, E. B.; Tao, Y. T.; Evall, J.; Whitesides, G. M.; Nuzzo, R. G. Formation of Monolayer Films by the Spontaneous Assembly of Organic Thiols from Solution onto Gold. *J. Am. Chem. Soc.* **1989**, *111*, 321−335.
(50) Puah, L. S.; Sedev, R.; Fornasiero, D.; Ralston, J.; Blake, T. Influence of Surface Charge on Wetting Kinetics. *Langmuir* **2010**, *26*, 17218−17224.
(51) Zhang, S.; Jamison, A. C.; Schwartz, D. K.; Lee, T. R. Self-Assembled Monolayers Derived from a Double-Chained Monothiol Having Chemically Dissimilar Chains. *Langmuir* **2008**, *24*, 10204−10208.
(52) Frey, B. L.; Corn, R. M.; Weibel, S. C. Polarization-Modulation Approaches to Reflection−Absorption Spectroscopy. *Handbook of Vibrational Spectroscopy*; John Wiley & Sons, Ltd., 2006.
(53) Casero, E.; Vazquez, L.; Parra-Alfambra, A. M.; Lorenzo, E. AFM, SECM and QCM as useful analytical tools in the characterization of enzyme-based bioanalytical platforms. *Analyst* **2010**, *135*, 1878−1903.
(54) Schneider, T. W.; Buttry, D. A. Electrochemical Quartz Crystal Microbalance Studies of Adsorption and Desorption of Self-Assembled Monolayers of Alkyl Thiols on Gold. *J. Am. Chem. Soc.* **1993**, *115*, 12391−12397.
(55) Rana, S.; Bajaj, A.; Mout, R.; Rotello, V. M. Monolayer Coated Gold Nanoparticles for Delivery Applications. *Adv. Drug Delivery Rev.* **2012**, *64*, 200−216.
(56) Vilar, M. R.; Botelho do Rego, A. M.; Ferraria, A. M.; Jugnet, Y.; Noguès, C.; Peled, D.; Naaman, R. Interaction of Self-Assembled Monolayers of DNA with Electrons: HREELS and XPS Studies. *J. Phys. Chem. B* **2008**, *112*, 6957−6964.
(57) Petrovykh, D. Y.; Kimura-Suda, H.; Whitman, L. J.; Tarlov, M. J. Quantitative Analysis and Characterization of DNA Immobilized on Gold. *J. Am. Chem. Soc.* **2003**, *125*, 5219−5226.
(58) Mankos, M.; Persson, H. H. J.; N'Diaye, A. T.; Shadman, K.; Schmid, A. K.; Davis, R. W. Nucleotide-Specific Contrast for DNA Sequencing by Electron Spectroscopy. *PLoS One* **2016**, *11*, No. e0154707.
(59) Luderer, F.; Walschus, U. Immobilization of Oligonucleotides for Biochemical Sensing by Self-Assembled Monolayers: Thiol-Organic Bonding on Gold and Silanization on Silica Surfaces. In *Immobilisation of DNA on Chips I*; Wittmann, C., Ed.; Springer: Berlin, Heidelberg, 2005; pp 37−56.
(60) Lahiri, J.; Isaacs, L.; Grzybowski, B.; Carbeck, J. D.; Whitesides, G. M. Biospecific Binding of Carbonic Anhydrase to Mixed SAMs Presenting Benzenesulfonamide Ligands: A Model System for Studying Lateral Steric Effects. *Langmuir* **1999**, *15*, 7186−7198.
(61) Osicka, J.; Ilčiková, M.; Popelka, A.; Filip, J.; Bertok, T.; Tkac, J.; Kasak, P. Simple, Reversible, and Fast Modulation in Superwettability, Gradient, and Adsorption by Counterion Exchange on Self-Assembled Monolayer. *Langmuir* **2016**, *32*, 5491−5499.
(62) Šponer, J.; Mladek, A.; Sponer, J. E.; Svozil, D.; Zgarbova, M.; Banas, P.; Jurecka, P.; Otyepka, M. The DNA and RNA Sugar-Phosphate Backbone Emerges as the Key Player. An Overview of Quantum-Chemical, Structural Biology and Simulation Studies. *Phys. Chem. Chem. Phys.* **2012**, *14*, 15257−15277.

DOI: 10.1021/acsami.8b12244
ACS Appl. Mater. Interfaces 2018, 10, 40890−40900